In-situ estimation of soil hydraulic and hydrodispersive properties by inversion of Electromagnetic Induction measurements and soil hydrological modelling

Giovanna Dragonetti[1,Ψ], Mohammad Farzamian[2,3,Ψ], Angelo Basile[4], Fernando Monteiro Santos[3], Antonio Coppola[5,6]

[1]Mediterranean Agronomic Institute of Bari, Valenzano (BA), 70010, Italy

2Instituto Nacional de Investigação Agrária e Veterinária, Oeiras, 2780-157, Portugal

[3]Instituto Dom Luiz, Faculdade de Ciências da Universidade de Lisboa, Lisboa, 1749-016, Portugal

[4]Institute for Mediterranean Agricultural and Forestry Systems, National Research Council, Portici (NA), 80055, Italy

[5]School of Agricultural, Forestry, Food and Environmental Sciences, University of Basilicata, Potenza, 85100, Italy

[6]Department of Chemical and Geological Sciences, University of Cagliari, Cagliari, 09124, Italy

Ψ These authors contributed equally to this work.

Correspondence: Mohammad Farzamian (mohammad.farzamian@iniav.pt) and Giovanna Dragonetti (dragonetti@iamb.it)

ABSTRACT

Soil hydraulic and hydrodispersive properties are necessary for modelling water and solute fluxes in agricultural and environmental systems. Despite the large efforts in developing methods (e.g. lab-based, pedotransfer functions), their characterization at applicative scales is still an imperative requirement. Accordingly, this paper proposes a non-invasive in situ method integrating Electromagnetic Induction (EMI) and hydrological modelling to estimate soil hydraulic and transport properties at the plot scale. To this aim, we carried out two sequential water infiltration and solute transport experiments and conducted time-lapse EMI surveys using a CMD

mini-Explorer to examine how well this methodology can be used to i) monitor water content dynamic after irrigation and to estimate the soil hydraulic van Genuchten–Mualem parameters from the water infiltration experiment and ii) to monitor solute concentration, and to estimate solute dispersivity from the solute transport experiment. We then compared the obtained results to those estimated by direct Time Domain reflectometry (TDR) and tensiometer probes measurements. The EMI significantly underestimated the water content distribution observed by TDR, but the water content evolved similarly over time. This introduced two main effects on soil hydraulic properties obtained by the two methods: i) Similar water retention curve shapes, but underestimated saturated water content from the EMI method, resulting in a scaled water retention curve when compared with the TDR method; the EMI-based water retention curve can be scaled by measuring the actual saturated water content at the end of the experiment with TDR probes or by weighing soil samples; ii) almost overlapping hydraulic conductivity curves, as expected when considering that the shape of the hydraulic conductivity curve primarily reflects changes in water content over time. Nevertheless, EMI-based estimations of soil hydraulic properties and transport properties were found to be fairly accurate in comparison to those obtained from direct TDR measurements and tensiometer probes measurements.

1. INTRODUCTION

Dynamics agro-hydrological models are more and more used for interpreting and solving agro-environmental problems (Hansen et al., 2012; Coppola et al., 2015; Kroes et al., 2017; Coppola et al., 2019). The soil hydrological component of these models is frequently based on mechanistic descriptions of water and solute fluxes in soils. Richards equation (RE) for water flow and Advection-Dispersion equation (ADE) for solute transport is generally accepted to apply at a local

scale (plot scale, for example). Solving RE requires the determination of the hydraulic properties, namely the water retention curve relating the soil water content, θ, to the soil water pressure head, h, and the hydraulic conductivity curve, relating the hydraulic conductivity, K to either the water content, θ or the pressure head, h. Similarly, ADE requires the dispersivity, λ, to be also known. In the last decades several laboratory and in-situ methods have been developed for characterizing soil hydraulic properties (e.g. Dane and Topp, 2020) and dispersive properties (e.g. Vanderborght and Vereecken, 2007). Lab-based characterizations may be carried out under more controlled conditions. Nevertheless, for simulating water and solute dynamics in the real field context, the in-situ methods are obviously more representative than the lab ones. This is firstly related to the size of the volume investigated, which has to appropriately represent the heterogeneity of the medium being studied (Wessolek et al., 1994; Ellsworth et al., 1996; van Genuchten et al., 1999; Inoue et al., 2000). Actually, a water flow process observed in situ will be influenced by the heterogeneities (stones, macropores, etc.) found in the field. This is the main limitation of the relatively small soil columns generally analysed in the laboratory. By contrast, an in-situ characterization method, for example the well-known instantaneous profile method (Watson et al., 1966), can catch the hydraulic properties which are effective in describing the flow process observed in-situ. This will also depend on the measurement scale (the size of the plot) and on the observation scale of the sensors used. These issues have been dealt with in detail for example in Coppola et al. (2012; 2016) and in Dragonetti et al., (2018). Besides, the experimental boundary conditions used to carry out the hydraulic characterization in lab and in-situ may also induce a different shape of the hydraulic properties as determined in the lab and in-situ (Basile et al., 2006).

In-situ methods typically evaluate soil hydraulic properties by monitoring an infiltration and/or a redistribution water flow process (Watson et al., 1966). Similarly, in situ methods for

72 determining hydro-dispersive parameters are generally based on monitoring of mixing processes
73 following pulse or step inputs of a tracer on either large plots or along field transect (Severino et
74 al., 2010; Coppola et al., 2011; Vanderborght and Vereecken, 2007). Inverse modelling is
75 frequently used to estimate the hydraulic and transport parameters simultaneously (e.g. Šimůnek
76 et al., 1998a; Abbasi et al., 2003; Groh et al., 2018). Yet, even by shortening the measurement
77 procedure by simplified assumptions (e.g. Sisson and van Genuchten 1991; Basile 2006) all in-
78 situ methods for the characterization of the whole soil profile remain extremely difficult to
79 implement also because they generally require installing sensors at different depths (e.g. TDR
80 probes, tensiometers, access tubes for neutron probe) which are cumbersome and may induce soil
81 disturbance, unless the installation is made much earlier than the experiment, to at least partly
82 allowing the soil to recover through several wetting-drying cycles its natural structure.

83 In this direction, geophysical non-invasive methods based on the electrical resistivity
84 tomography (ERT) and Electromagnetic Induction (EMI) techniques represent a promising
85 alternative to traditional sensors for soil hydraulic and transport parameters assessment. Many
86 researchers have used the time-lapse ERT data (e.g. Binley et al., 2002; Kemna et al., 2002; Singha
87 and Gorelick, 2005) to monitor water content and saline tracer in the field. The dependence of soil
88 electrical conductivity on soil water content and concentration is the key mechanism that permits
89 the use of time-lapse ERT to monitor water and solute dynamics in time-lapse mode along a soil
90 profile, by relating resistivities to water contents and solute concentration distributions through
91 empirical or semi-empirical relationships (e.g. Archie, 1942) or established in-situ relationships
92 (e.g. Binley et al., 2002).

93 Electromagnetic induction (EMI) sensors may be also used as they allow for monitoring water
94 and solute propagation through a soil profile by simply moving the sensor above the soil surface

without the need to install electrodes, as required by ERT technique. An EMI sensor provides measurements of the depth-weighted apparent electrical conductivity (σ_a) according to the specific distribution of the bulk electrical conductivity (σ_b), as well as the depth response function of the sensor used (McNeill, 1980). σ_a obtained from EMI sensors have been used to map the geospatial and temporal variability of the soil water content and salinity (Corwin and Lesch, 2005; Bouksila et al. 2012; Saeed et al., 2017). However, monitoring the propagation of the water and solutes with depth along a soil profile (as during a water infiltration or a solute transport experiment) requires the distribution of the σ_b distribution with depth to be known over time, which can be obtained by inversion of the σ_a observations from the EMI sensor (see for example, Hendrickx et al., 2002; Lavoué et al., 2010; Deidda et al., 2014; Von Hebel et al., 2014; Dragonetti et al., 2018; Moghadas et al., 2019; Farzamian et al., 2019a; Zare et al. 2020; Mclachlan et al. 2020). More recently, this inversion has been facilitated by the development of multi-coil EM sensors which are designed to collect σ_a at multiple coil spacing and orientations simultaneously in one sensor reading. This allows a rapid investigation of the soil's electrical conductivity at several depth ranges to obtain soil water content (Huang et al., 2016; Whalley et al., 2017) and solute concentrations (Paz et al., 2020; Gomez Flores et al., 2022) quickly and cheaply. However, the potential of EMI sensors to assess soil hydraulic and hydro-dispersive parameters has not been yet studied due to the lack of high-resolution and well-controlled experiments, required to catch the complexity of water flow and transport process during infiltration experiments.

With these premises, in this paper we propose a procedure based on a sequence of water infiltration and solute transport experiments, both monitored by an EMI sensor, with the objective of estimating in-situ the parameters of soil hydraulic properties and the dispersivity of a soil profile with a non-invasive EMI sensor and relatively short experiments at the plot scale. The sequence

of water and solute infiltration has the main aim to discriminate the contribution of the water content and the soil solution electrical conductivity to the EMI-based σ_b. All the EMI data will be analysed by a hydrological model within a so-called uncoupled framework. The goodness of the adopted approach will be evaluated by comparing the EMI-based hydraulic and hydrodispersive properties to those obtained from in-situ TDR and tensiometer measurements. The aim is to explore an approach that does not need sensors installation and minimise data necessary for the in-situ assessment of soil hydraulic and hydrodispersive properties.

2. HYDRO-GEOPHYSICAL UNCOUPLED APPROACH

Figure 1 provides a schematic view of a six-step (+ one step for comparison) procedure, based on an uncoupled approach (Camporese et al., 2015) which will be adopted in this work to estimate the soil hydraulic and hydrodispersive properties using the data obtained from the EMI sensor. All the steps summarised below will be described in detail in the Materials and Methods section.

(i) Inversion of time-lapse σ_a EMI data obtained during (i) a water infiltration experiment, hereafter 1st experiment, and (ii) a subsequent solute transport experiment, hereafter 2nd experiment, to generate EMI-based σ_b distributions for each experiment;

(ii) Laboratory calibration of the relationship θ-σ_b-σ_w in order to convert σ_b distributions to water content, θ, (1st experiment) and to soil solution electrical conductivity, σ_w, and therefore solute concentrations, *C*, (2nd experiment);

(iii) Converting the σ_b distributions obtained from the 1st experiment to water content distributions, using the θ-σ_b-σ_w relationship, to be used in the next numerical simulation step;

(iv) Numerical simulation, by using the HYDRUS-1D model (Šimůnek et al., 1998b), of the 1st experiment in order to estimate the van Genuchten-Mualem (vG-M) parameters through an inversion procedure based on the water contents inferred from step (iii);

(v) Conversion of the σ_b distributions obtained from the 2nd experiment to solute concentration distribution in order to estimate longitudinal dispersivity, λ. In this step, σ_w distribution was estimated by using the laboratory θ-σ_b-σ_w calibration. The θ distribution in the 2nd experiment was simulated based on the vG-M parameters obtained in step (iv). This is a crucial step in the proposed procedure, as it allows to discriminate the contribution of the soil water electrical conductivity, and thus of the solute concentration, to the σ_b EMI readings during the 2nd experiment. The σ_w distributions were thus converted to solute concentration by a simple standard lab-based solute specific σ_w-*C* relationship;

(vi) Numerical simulation of the second solute infiltration process in order to estimate λ through an inversion procedure based on the concentrations obtained from step (v).

(vii) An alternative dataset of θ and σ_b obtained from direct TDR measurements, as well as tensiometer pressure head (h) readings, collected during the two experiments, allowed us to obtain independent hydraulic and hydrodispersive properties (hereafter TDR-based for sake of simplicity) to be used as a reference to evaluate the EMI-based parameter estimation (see the horizontal grey box in Fig. 1).

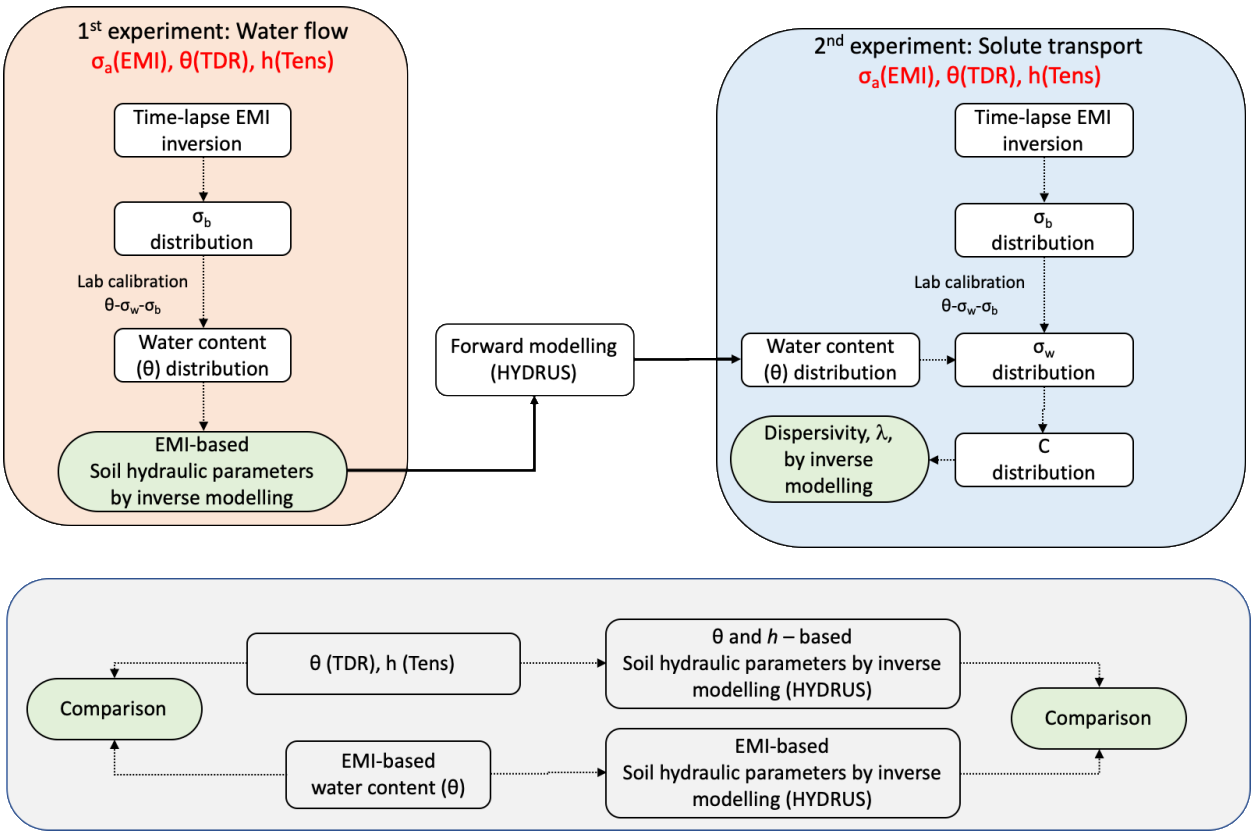

Figure 1: Schematic diagram of the proposed Hydro-Geophysical uncoupled approach

3. MATERIAL AND METHODS

3.1. Study area

The experiment was performed at the Mediterranean Agronomic Institute of Bari (CIHEAM-IAM), south-eastern coast of Italy. The study area is located at an altitude of 72 m with 41° 3' 13.251" N, a longitude of 16° 52' 36.274" E, with a typical Mediterranean climate with rainy winters and very hot dry summers. The soil is a Colluvic Regosol consisting of silty loam layers of an average depth of 70 cm on a shallow fractured calcareous rock. Two main horizons on the calcareous rock may be identified: an Ap horizon (depth 0-30 cm) and a Bw horizon (depth 30-70 cm). Scattered calcareous fragments are present due to the breaking and grinding of the bedrock

operated in the past by using heavy machinery in order to improve the soil structure and increase the soil depth for plantation

3.2. Experimental set-up

A layout of the experimental setup is shown in Fig. 2. The plot size is 4 × 4 m. Water was applied by using a drip irrigation system consisting of 20 lines, with drippers spaced 0.20 m and delivering a nominal flow rate of 10 l h^{-1}. Thus 400 drippers were installed, capable of delivering 4000 l h^{-1} on the whole plot. The dripper's grid spacing and the flow rate were selected to ensure that a 1D flow field rapidly developed after starting irrigation. The drip irrigation system was placed on a metallic grid to be easily moved away from the plot and whenever EMI measurements were taken on the ground soil.

Several months before starting the 1st experiment, after digging a small pit, eight three-wire TDR probes, 7 cm long, 2.5 cm internal distance, and 0.3 cm in diameter, were inserted horizontally at 2 depths − 20 and 40 cm, corresponding to the Ap and the Bw horizon − in the 4 corners of the experimental plot (at 1 m distance from the plot edge), as shown in Fig. 2. The pits for installing the sensors were refilled immediately, to leave some natural wetting and drying cycles to reproduce the original soil aggregation. Then, the plot was covered with a plastic sheet about four days prior to the start of the experiment to keep the plot under quasi-equilibrium conditions at the beginning of the experiment.

A Tektronix 1502C cable tester (Tektronix Inc., Baverton, OR) was used in this study, enabling simultaneous measurement of water content, θ, and bulk electrical conductivity, σ_b, of the soil volume explored by the probe (Robinson et al., 2003; Coppola et al., 2011; 2013). Furthermore, eight tensiometers were vertically inserted near each TDR probe to acquire water potentials by a

192 Tensicorder sensor (Hydrosense3 SK800). Both TDR probes and tensiometers were installed for
193 the evaluation of the EMI-based parameter estimation (step (vii)).

194 The experimental plot was firstly irrigated by using tap water with an electrical conductivity
195 of about 1 dS m^{-1} (1^{st} experiment). We applied eleven irrigations, each lasting about 3 minutes to
196 deliver about 180 l on the whole 16 m^2 plot for each irrigation (the volume was measured by a
197 flowmeter). Irrigations were separated by about a 1-hour shutoff. At each irrigation starting, due
198 to the short inertia of the irrigation system just after its switching on, for some seconds drippers
199 delivered less than 10 l h^{-1}. For each irrigation an average flow rate of about 0.375 cm min^{-1} was
200 applied, which generated a small ponding at the soil surface for a short time. Overall, an average
201 water volume of 2000 l was supplied.

202 The propagation of the wetting front along the soil profile was monitored by using an EMI
203 sensor (i.e. CMD mini-Explorer, GF Instruments, Czech Republic), positioned horizontally in the
204 middle of the plot (Fig. 2) in order to measure the apparent electrical conductivity, σ_a, in the soil
205 profile in VCP (vertical coplanar, i.e., horizontal magnetic dipole configuration) mode and then
206 HCP (horizontal coplanar, i.e., vertical magnetic dipole configurations) mode by rotating the probe
207 90° axially to change the orientation from VCP to HCP mode. The CMD Mini-Explorer operates
208 at 30 kHz frequency and has three receiver coils with 0.32, 0.71 and 1.18 m distances from the
209 transmitter coil, referred to hereafter as ρ32, ρ71, and ρ118. The manufacturer indicates that the
210 instrument has an effective depth range of 0.5, 1.0 and 1.8 m in the HCP mode, which is reduced
211 to half (0.25, 0.5, and 0.9 m) by using the VCP orientation. As a consequence, this EMI sensor
212 returns six different σ_a values (utilizing three offsets with two coil orientations) with each
213 corresponding to different depth sensitivity ranges. All measurements were performed five
214 minutes after each water pulse application by temporarily removing the irrigation grid and placing

the EMI sensor in the middle of the plot. The infiltration was also monitored by TDR probes and tensiometers in order to monitor the space-time evolution of water content, θ, pressure head, h, as well as bulk electrical conductivity, σ_b. The distance of the TDR probes and tensiometers to the middle of the plot was specifically designed to avoid any interference with the EMI measurements.

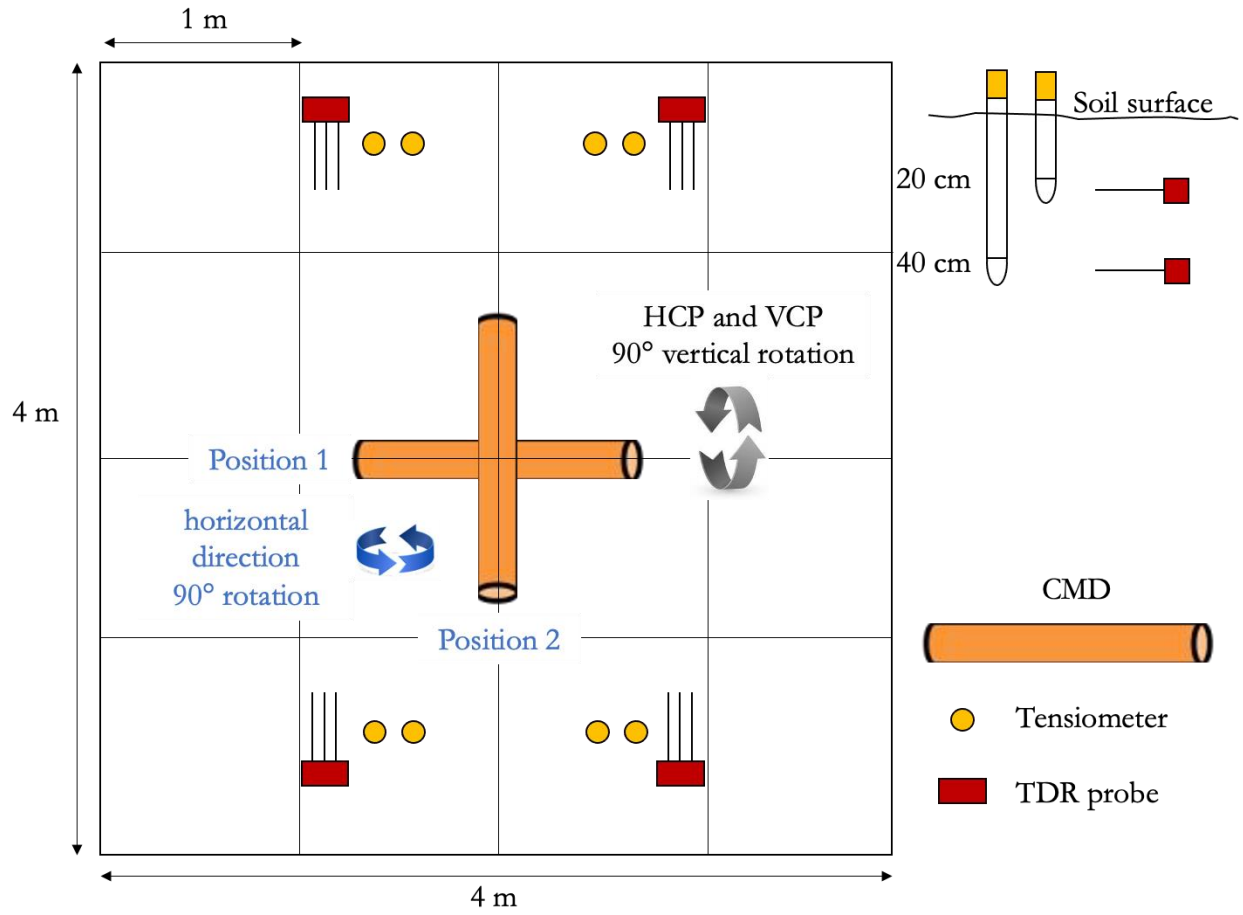

Figure 2. Layout of the experimental and monitoring set-up. HCP (horizontal coplanar) and VCP (vertical coplanar) are the vertical and horizontal dipolar orientations of the CMD probes, respectively.

At the end of the 1st experiment, the soil was allowed to dry and then covered with a plastic sheet to bring the distribution of water content along the profile similar to the initial one (observed

before the water infiltration test). Afterward, a similar infiltration experiment (2^{nd}) was carried out but using saline water at an electrical conductivity of 15 dS m^{-1}, and obtained by mixing $CaCl_2$ into the tap water. Again, eleven saline water supplies were provided at intervals of about 1 h apart and a total volume of 2000 l saline water was supplied during the experiment. The propagation of the water and chloride during the 2^{nd} infiltration experiment was monitored similarly to the 1^{st} experiment using TDR probes, tensiometers, and the CMD Mini-Explorer sensor.

3.3. Site-specific calibration θ-σ_b-σ_w

The relationship between the bulk electrical conductivity (σ_b), the electrical conductivity of the soil solution soil water (σ_w), and the water content, were obtained by using the model proposed by Malicki and Walczak, (1999):

$$\sigma_w = \frac{\sigma_b - a}{(\varepsilon_b - b)(0.0057 + 0.000071\, S)} \quad (1)$$

where ε_b (-) is the dielectric constant, which is related to the water content and S is the sand content in percent. The parameters a = 3.6 dS m^{-1} and b = 0.11 were obtained in a laboratory experiment reported in Farzamian et al. (2021). Topp's equation was used to relate dielectric constant to the volumetric water content (Topp et al., 1980). The lab experiment for such a calibration is quite simple, fast, and standard procedure on reconstructed soil samples. An additional linear calibration, obtained by using solutions at different concentrations of calcium chloride was used to relate soil water concentrations of chloride, Cl^-, to σ_w.

3.4. Inversion of time-lapse EMI σ_a data

Time-lapse σ_a data obtained during the experiments were inverted using a modified inversion algorithm proposed by Monteiro Santos et al. (2004) to obtain σ_b distribution in time. The aim of the inversion is to minimize the penalty function that consists of a combination between the observations' misfit and the model roughness (Farzamian et al., 2019b). The earth model used

in the inversion process consists of a set of 1D models distributed according to the number of time-lapse measurements. All the models have the same number of layers (i.e. 7) whose thickness is kept constant. The selected depths of layers are 10, 20, 30, 40, 55, 75 and 180 cm. The number and thickness of layers were selected based on several factors including the number of σ_a measurements (i.e., 6), effective depth range of HCP and VCP modes (i.e., 5 of 6 measurements have an effective depth of less than 1m), and site specifications (i.e., the large variability of conductivity of the soil profile over a resistive bedrock). The parameters of each model are spatially and temporally constrained using their neighbours through smooth conditions. The forward modelling is solved based on the full solution of the Maxwell equations (Kaufman and Keller, 1983) to calculate the σ_a responses of the model. The inversion algorithm is Occam-regularization and the objective function was developed based on Sasaki, (2001). Therefore, the update of the parameters, in an iterative process are calculated solving the system:

$$[(J^T J + \eta C^T C)] \delta p = J^T b \quad (2)$$

where δp is the vector containing the corrections applied to the parameters (logarithm of block conductivities, p_j) of an initial model, b is the vector of the differences between the logarithm of the observed and calculated σ_a [$b_i = \ln(\sigma_a^o/\sigma_a^c)_i$], J is the Jacobian matrix whose elements are given by (σ_j/σ_{ai}^c) $(\partial\sigma_{ai}^c\ \partial\sigma_j)$, the superscript T denotes the transpose operation, and η is a Lagrange multiplier that controls the amplitude of the parameter corrections and whose best value is determined empirically. The elements of matrix C are the coefficients of the values of the roughness of each 1D model, which is defined in terms of the two neighbour's parameters and the constraint between the parameters of the different models on time. In this regard and in the temporal 1D experiment, each cell is constrained spatially by its vertical neighbours, while the temporal constraints are imposed using its lateral neighbours. An iterative process allows the final

models to be obtained, with their response fitting the data set in a least-square sense. In terms of η, generally, large values will produce smooth inversion results with smoother spatial and temporal variations.

We performed several syntenic tests to determine how well the proposed inversion algorithm can predict spatiotemporal variability of σ_b and to fine-tune the regularization parameters. The syntenic scenarios were selected based on spatiotemporal variability of σ_a in the HCP and VCP modes, the site specification (e.g. shallow bedrock) and the expected evolution of conductive zone due to water and saline water infiltrations.

3.5. Numerical simulation of water flow and chloride transport in soil

The water and the chloride propagation monitored during the experiments were simulated by using the HYDRUS-1D model (Šimůnek et al., 1998b). HYDRUS-1D simulates water flow and solute transport by solving the Richards equation and the Advection-Dispersion equation, respectively.

Richards equation can be written for one-dimensional, unsaturated, non-steady state flow of water in the vertical direction as follows:

$$C_w(\theta)\frac{\partial h}{\partial t} = \frac{\partial}{\partial Z}\left[K(h)\frac{\partial h}{\partial Z} + K(h)\right] \quad (3)$$

where $C_w(\theta)$, the water capacity, is the slope of the water retention curve, θ is the volumetric water content [L^3L^{-3}], h is the soil water pressure head [L], $K(h)$ is the unsaturated hydraulic conductivity [LT^{-1}].

The Advection-Dispersion equation governing the transport of a single non-reactive and non-adsorbed (a tracer, chloride in this case) ion in the soil can be written as:

293 $$\frac{\partial(\theta C)}{\partial t} = \frac{\partial}{\partial z}\left[\theta D \frac{\partial C}{\partial z} - qC\right] \quad (4)$$

294 where q is the darcian flux, C is the solute concentration in the liquid phase [ML^{-3}], D (L^2T^{-1}) is
295 the effective dispersion coefficient, which can be assumed to come from a combination of the
296 molecular diffusion coefficient, D_{diff} (L^2T^{-1}) and the hydrodynamic dispersion coefficient, D_{dis}
297 (L^2T^{-1}):

298 $$D = D_{\text{diff}} + D_{\text{dis}} \quad (5)$$

299 where hydrodynamic dispersion is the mixing or spreading of the solute during transport due to
300 differences in velocities within a pore and between pores. The dispersion coefficient can be related
301 to the average pore water velocity $v=q/\theta$ through:

302 $$D = \lambda v \quad (6)$$

303 where λ [L] is the dispersivity, a characteristic property of the porous medium. To solve the
304 Richards equation (Eq. 3), the water retention function, θ(h), and the hydraulic conductivity
305 function, $K(h)$, must be defined. In this paper we adopted the van Genuchten-Mualem model (vG-
306 M), (van Genuchten, 1980):

307 $$S_e = [1 + (\alpha|h|)^n]^{-m} \quad (7)$$

308 $$K(h) = K_s S_e{}^{\tau}\left[1 - \left(1 - S_e{}^{1/m}\right)^m\right]^2 \quad (8)$$

309 In Eqs. 7 and 8, $S_e = \frac{(\theta-\theta_r)}{(\theta_S-\theta_r)}$ is the effective water saturation, θ_s the saturated water content, θ_r the
310 residual water content, α, n and m are fitting parameters with m taken as m=1-1/n, K_s is the
311 saturated hydraulic conductivity and τ is the pore-connectivity parameter.

312

3.6. Inverse estimation of soil hydraulic and solute transport parameters

The obtained EMI-based spatiotemporal distribution of σ_b during the 1st experiment was converted to the θ distribution in order to estimate the temporal evolution of θ during the infiltration process. These water content data were then used in an optimization procedure by using the HYDRUS-1D model, in order to estimate the hydraulic properties of the different horizons in the soil profile. The simulations were carried out by using the actual top boundary flux conditions during the experiment, including the irrigation events. For the bottom boundary, free drainage was considered. A simulation domain of 150 cm depth was considered. The same procedure was repeated using the direct measurements of θ and h inferred from TDR and tensiometers, respectively, in order to obtain independent hydraulic parameters (TDR-based estimation) to be compared to those inferred from EMI. A three-layer soil profile (0-25; 25-70; 70-150 cm), reflecting the actual pedological layering (i.e. Ap, Bw, and bedrock) was used in all simulations. In terms of the initial condition, a hydrostatic distribution of the pressure heads, h, was considered for the TDR-based simulations. On the other hand, the water content distribution, inferred from the first EMI survey (before irrigation) was considered for the EMI-based simulation.

As for the solute transport experiment, a HYDRUS-1D simulation was carried out with the EMI-based hydraulic properties obtained from the 1st experiment to simulate the water content distributions in correspondence with the EMI measurement times. The simulations of water infiltration and solute transport in the 2nd experiment were carried out by using the top boundary fluxes conditions applied during the 2nd experiment along with the same simulation domain, three-layer soil profile, and the bottom boundary and equilibrium initial conditions described above. Thus, for each monitoring time, we had available the σ_b distributions obtained from the EMI and the θ distributions coming from the HYDRUS-1D simulations. These distributions allowed us to

336 estimate as many σ_w (and thus *C*) distributions by using the θ-σ_b-σ_w relationship obtained in the
337 laboratory. These *C* distributions were used in a new HYDRUS-1D simulation to estimate the
338 longitudinal dispersivity of the investigated soil. The simulated concentrations, with the optimized
339 dispersivity, λ, were compared to those obtained from the TDR and tensiometer data.

340

341 ## 4. RESULTS AND DISCUSSION

342 ### 4.1. Water infiltration – 1st experiment

343 #### 4.1.1. *Time-lapse σ_a data and estimation of σ_b distribution*

344 Figure 3 shows the σ_a values observed during the water infiltration experiment. Both VCP
345 and HCP modes show a relatively similar pattern of σ_a values with ρ32 and ρ118 being the highest
346 and lowest respectively. HCP mode shows higher values compared to the VCP mode in the same
347 receivers. This pattern of σ_a distribution suggests the presence of a conductive zone over a resistive
348 zone which is expected in this experiment as a result of the waterfront being infiltrated into the
349 soil profile and the presence of a resistive bedrock. In terms of temporal σ_a variabilities, the σ_a
350 increases consistently in both VCP and HCP modes during the first three hours of the experiment.
351 Afterward, σ_a did not change significantly toward the end of the experiment. The range of σ_a
352 variations is relatively small in both VCP and HCP modes with the former in the 10-30 mS m^{-1}
353 range and the latter in the 10-50 mS m^{-1} range.

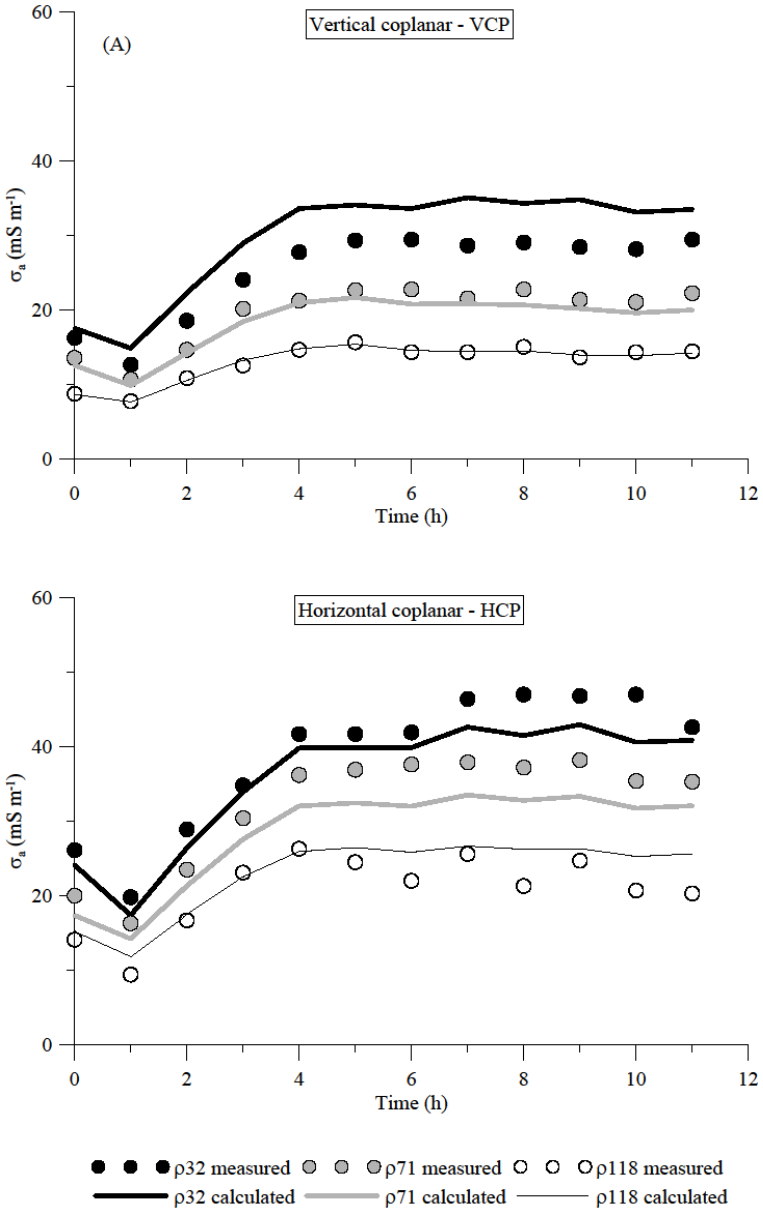

Figure 3: σ_a values observed during the water infiltration experiment. (A) VCP, (B) HCP. The symbols represent the measured data whereas the lines represent the values calculated after the inversion.

354 Prior to the inversion of σ_a data we fine-tuned the regularization parameter, η, as discussed
355 in 3.4. the results of several synthetic tests (not shown here) suggest that a value of η between 1 to

5 provides a better result in resolving the spatio-temporal σ_b distributions in both experiments. Figure 4 depicts the time-lapse σ_b modelling results of σ_a shown in Fig. 3. The model shows clearly the evolution of the conductive zone into the soil profile shortly after the irrigation started as expected from the σ_a data. The resistive zone beneath a conductive zone corresponds to the bedrock layer in the experimental plot. The σ_b of the resistive zone remains below 5 mS m^{-1} and does not vary significantly during the experiment, while, in contrast, the σ_b of the upper layers increased significantly from an average of 20 mS m^{-1} at the beginning of the experiment to more than 50 mS m^{-1} after the 5^{th} irrigation. The conductivity of this zone does not increase largely since then, suggesting that the upper soil is fairly saturated after the 5^{th} irrigation. The calculated response of this model was shown in Fig. 3. There is a fairly good agreement between σ_a measurements and model response, however, a slight shift can be noticed in the ρ32- VCP mode and ρ71- HCP mode between data and model response. This shift can be due to several reasons such as i) the instrumental drift of the EMI sensor, ii) the large spatiotemporal variability of soil electrical conductivity in this experiment as well as smoothness constraint performed in the inversion process to stabilize the inversion process which make it difficult to resolve the sharp changes, and iii) the choice of initial model.

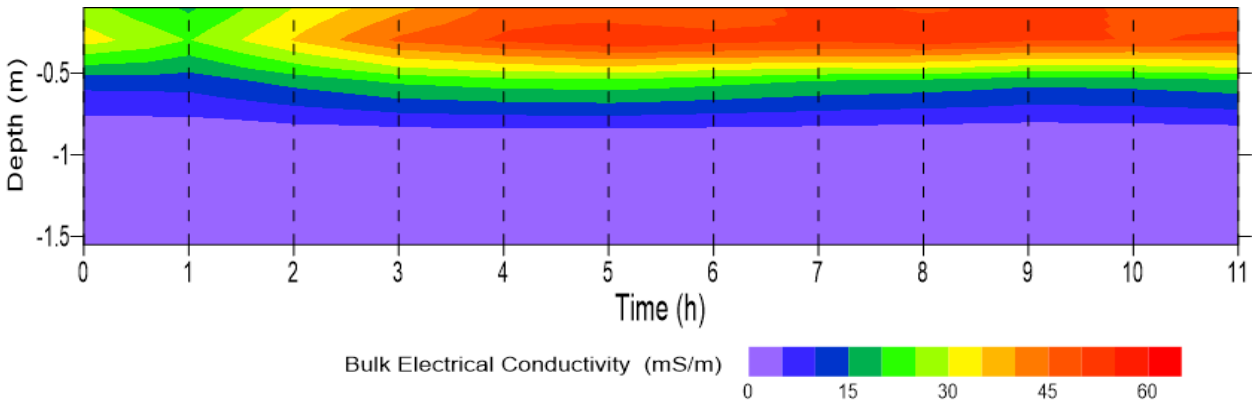

Figure 4. Time evolution of bulk electrical conductivity (σ_b) distribution with depth during the water infiltration experiment.

375 4.1.2. *Comparison between TDR-based and EMI-based σ_b and θ distributions*

376 Figure 5 shows the temporal σ_b changes inferred from TDR and EMI observations at two
377 depths, 20 and 40 cm. As reported by some authors (e.g. Coppola et al., 2016; Dragonetti et al.,
378 2018), both techniques provide σ_b estimations but a direct comparison between σ_b by TDR and
379 EMI is not straightforward due to different observation volumes of the two sensors. However, this
380 comparison can be used as a means to investigate the consistency of the σ_b trends and to provide
381 an insight into the uncertainty associated with the EMI survey and inversion process in resolving
382 the water infiltration process into the soil profile. Note that the average of TDR measurements in
383 four corners at depths of 20 and 40 cm were considered both in this comparison and in the inversion
384 procedure. The average values and the standard deviation of TDR measurements were presented
385 in Fig. 5.

386 Focusing on the σ_b series inferred from both TDR observations and EMI inversion, a
387 similar time pattern of σ_b variability is evident, but in general, the EMI model underestimates the
388 σ_b obtained by TDR. A better agreement was observed at 20 cm in terms of both absolute σ_b values
389 and trend (r=0.94; Mean Error=10.1 mS m^{-1}). In contrast, at 40 cm, the mismatch between TDR
390 observations and EMI inversions becomes larger at the end of the experiment. The EMI σ_b values
391 – especially at 40 cm depth – remain rather invariant in the last part of the infiltration experiment.
392 The general outcome that for both layers the EMI σ_b values underestimate the TDR σ_b
393 measurements has been frequently found in the literature (e.g. von Hebel et al., 2014; Coppola et
394 al., 2015; Dragonetti et al., 2018; Visconti and de Paz, 2021). Furthermore, TDR measurements
395 show a low local variability, as depicted in Fig. 5 by the error bars reporting the standard deviation
396 of the σ_b as measured by the four TDR probes.

Figure 6 shows the evolution of θ at the same two depths, 20 and 40 cm as observed by TDR and EMI sensors. TDR provides the direct in-situ measurement of θ. In contrast in order to estimate θ from EMI observation, σ_b values extracted at these depths (Fig. 4) were converted to θ by the calibration performed in the laboratory, as detailed in Farzamian et al., (2021). A rapid increase of θ is visible shortly after injection in both EMI-based and TDR-based measurements. The EMI-based θ estimation is able to detect the similar water content evolution (similar water content differences over time) observed by TDR measurements but at a different water content level. Specifically, EMI water contents were lower than the TDR ones but the two series showed a quasi-parallel evolution at 20 cm depth (r=0.98; Mean Error=0.09 cm^3 cm^{-3}), while diverging for longer times at 40 cm depth (r=0.60; Mean Error=0.17 cm^3 cm^{-3}).

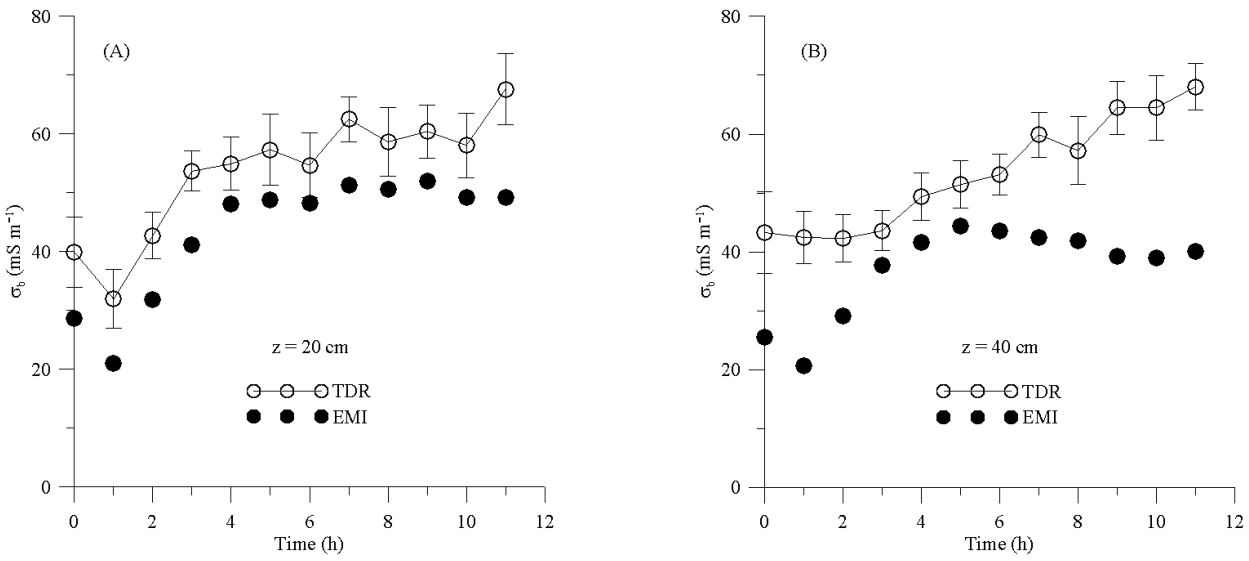

Figure 5. σ_b evolution estimated from the TDR and EMI measurements at 20 cm (A) and 40 cm (B) depths. The vertical bars represent the standard deviation of the measurements obtained by the four TDR sensors.

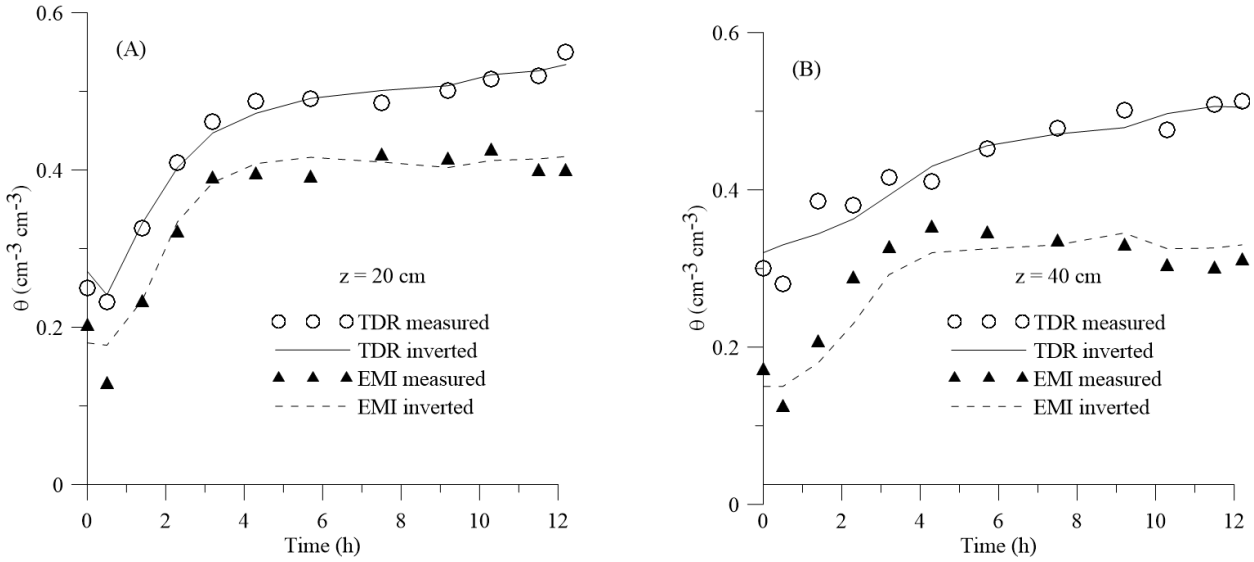

Figure 6. Evolution of θ measured by TDR (circles) and estimated from EMI measurements (triangles) at 20 cm (A) and 40 cm (B) depths. Continuous lines for TDR and dashed lines for EMI refer to the estimation obtained by the inversion procedure of the water infiltration process (see Sect. 4.1.3 below).

4.1.3. *Estimation of hydraulic properties*

In order to estimate hydraulic properties parameters, an inversion procedure was carried out applying HYDRUS-1D. The first set of hydraulic parameters was obtained by using the soil water contents measured by TDR and the pressure heads measured by tensiometers as measured data in the objective function for the optimization procedure (TDR-based). The second set of hydraulic parameters was obtained by using the soil water contents estimated by EMI measurements as measured data (EMI-based). The inversion simulations were carried out by fixing θ_r=0 and τ=0.5, while θ_s, α, n and K_s were optimized for both the Ap and the Bw layers. The hydraulic properties of the bedrock were already known and fixed to θ_r=0.068, θ_s=0.354, α=0.055, n=3.67, τ=0.5 and K_s=19.02 according to Caputo et al. (2010; 2015). We want to stress here that

429 an a-priori characterization of the bedrock layer is not essential and the proposed procedure holds
430 independently on the presence of bedrock. We could have treated the bedrock layer as any other
431 layer in the soil profile, but inserting TDR probes and tensiometers into bedrock presents
432 difficulties. Therefore, we decided to fix the bedrock parameters to the values already available
433 from independent measurements. In different soils with either deeper or absent bedrock, we could
434 have inserted TDR probes into deeper layers of the profile and applied the procedure to any of
435 them.

436 In the inversion procedure, the parameters were determined separately for each horizon of
437 the profile (Abbaspour et al., 1999). First, the parameters for the topsoil were estimated and these
438 parameters were then treated as known for the second layer estimation. Despite the water content
439 development in one layer is not independent from the hydraulic properties of the other layers when
440 long-time evolution is considered, in the case of a relatively short infiltration event as used here,
441 this approach makes parameter estimation of multi-layered profiles feasible. It should be noted
442 that in the case of the TDR-based estimations, optimization involved both measured water contents
443 and pressure head data, whereas the EMI-based estimations only involved "measured" water
444 contents.

445 Figure 6 reports a comparison between water contents measured (symbols) and estimated
446 (lines) by the inversion procedure. The θ evolution was properly estimated at 20 cm depth in both
447 approaches. It is worth noting here that, despite the differences in the absolute value of the water
448 contents, a clear parallel behaviour of the two curves was observed, suggesting similar water
449 content changes over time. A lower agreement was obtained at 40 cm but still reproduced similar
450 water content changes over time. This is a crucial point in this paper, as the parallel behaviour of

451 the water content evolution will explain the similar shape of hydraulic properties we found for the
452 TDR and EMI-based estimations (see Figure 8).

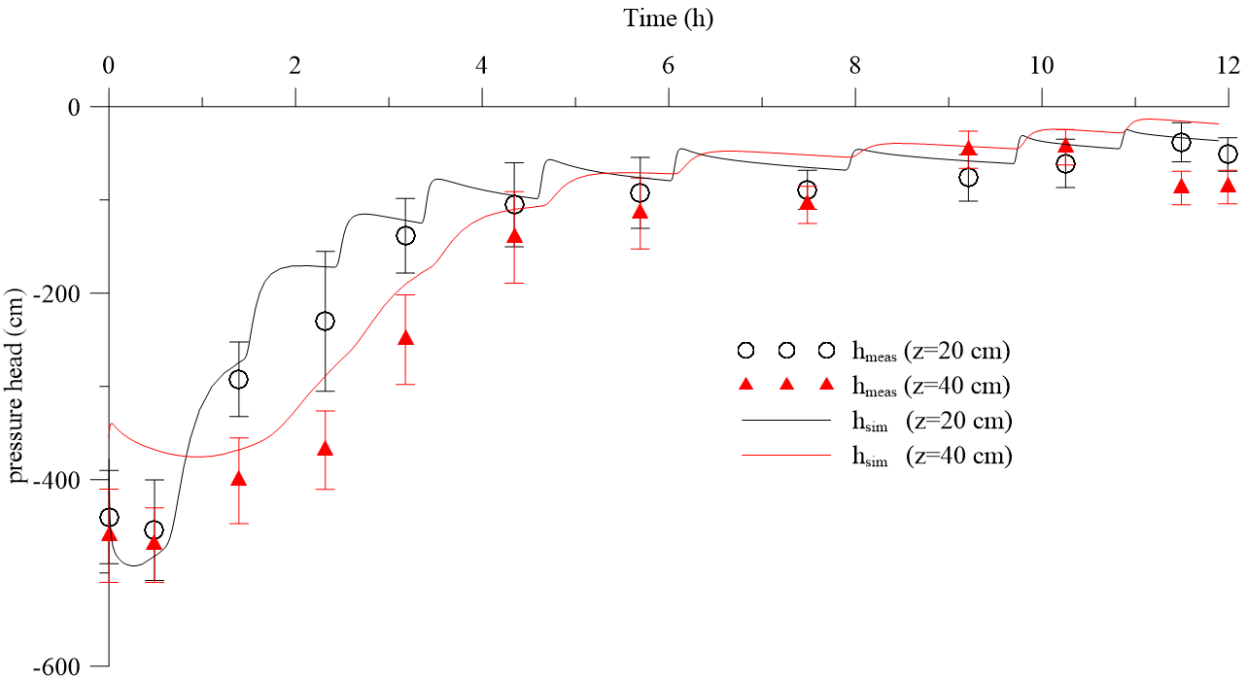

453

454 Figure 7. Evolution of pressure head at 20 and 40 cm depth measured by tensiometers (symbols)
455 and estimated by the inversion procedure (lines) of the water infiltration process. The vertical bars
456 represent the standard deviation of the measurements obtained by the four tensiometers.

457

458 Similarly, in Fig. 7 the measured (points) and estimated (lines) values of pressure heads
459 are shown. The simulated values of pressure head well follow the measured one (r=0.950 at 20 cm
460 and r=0.986 at 40 cm depth). Furthermore, the error bars, reporting the standard deviation of the
461 pressure head as measured by the four tensiometers, overlap when the profile is wet (i.e. after the
462 6th irrigation) and separate during the wetting process.

463 Table 1 reports the parameters of the hydraulic functions, estimated for the first two
464 horizons and Fig. 8 reports the water retention curves and the hydraulic conductivity curves
465 corresponding to the parameters shown in table 1 for a better comparison between TDR-based and

EMI-based hydraulic properties assessment. Compared to the Ap horizon, higher K_s and lower n values were found for the Bw horizon. This may be explained by considering that tillage in the Ap horizon changes the geometry of the porous system, by reducing the structural pores, responsible of the lower K_s for Ap, and increasing the textural pores, explaining the higher n value for Ap. Note in the table the high values of n and K_s for the bedrock, which indicate a high conductive porous medium. It is possible to explain this by considering that the bedrock is fractured calcareous, which, contrary to expectation, does not impede water flow.

Table 1. vG-M Hydraulic parameters (Eqs. 7 and 8) and dispersivity, λ (Eq. 6) as estimated for Ap and Bw horizons, and fixed for the bedrock layer.

Soil hydraulic and transport parameters*		Ap		Bw		Bedrock
		TDR-based	EMI-based	TDR-based	EMI-based	Fixed a-priori
θ_s	[$cm^3\ cm^{-3}$]	0.54	0.45	0.52	0.45	0.354
α	[cm^{-1}]	0.006	0.003	0.009	0.007	0.055
n	[-]	1.70	1.54	1.50	1.41	3.67
k_s	[$cm\ min^{-1}$]	0.06	0.02	0.28	0.29	19
λ	[cm]	10	12	0.5	0.8	30

* For all horizons θ_r=0 and τ=0.5.

As for water retention, the TDR and EMI water retention curves showed similar shapes but with slightly different saturated water contents. As discussed earlier, the lower saturated water content is not surprising for the EMI-based estimation due to the overall underestimation of water content. The two curves almost overlapped once scaling the EMI curve by the ratio of the saturated water contents. Obviously, this result is consistent with the underestimation of EMI-based θ distributions as shown in Fig. 6.

As for the hydraulic conductivity, TDR-based and EMI-based hydraulic conductivity curves at both 20 and 40 cm appear to almost overlap, with similar saturated hydraulic conductivity and curve shape. This result is expected because the shape of hydraulic conductivity curve is mainly explained by the variation of θ and not the absolute value of θ. It is worth mentioning that the same top boundary flux and different water contents in the soil profile provided similar EMI-based and TDR-based hydraulic conductivity. These conditions led to two different water flow processes, with simulations predicting higher water stored in the soil profile and lower downward fluxes (data not shown) when TDR-based results are compared to the EMI-based results.

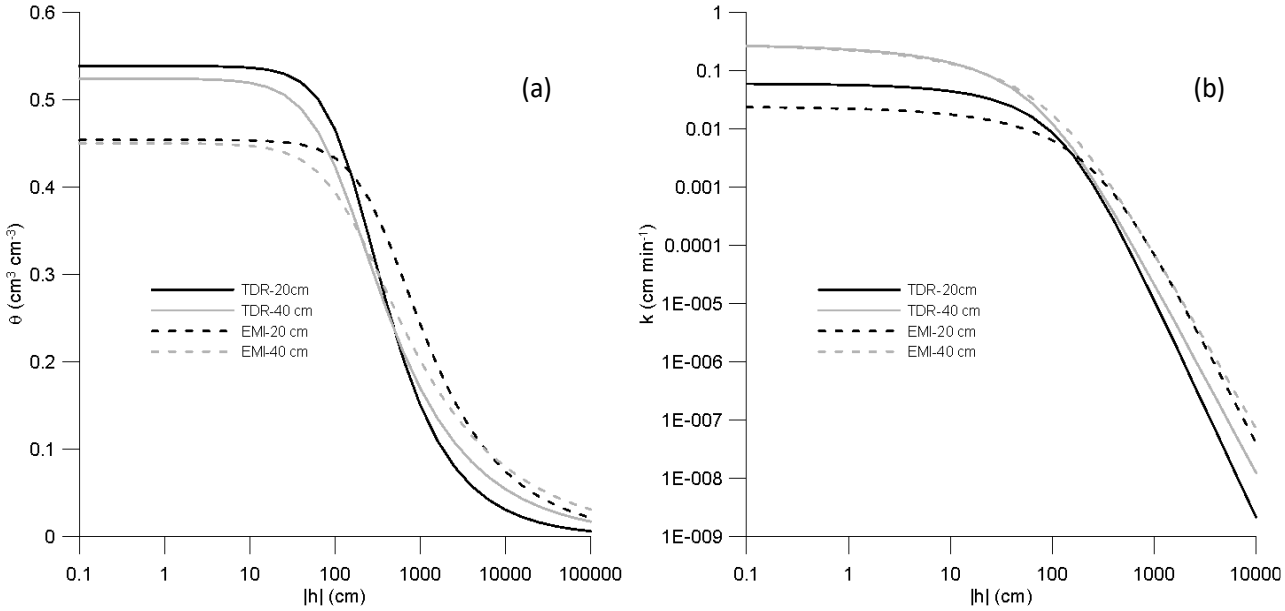

Figure 8. Soil water retention (A) and unsaturated hydraulic conductivity (B) curves, estimated from the TDR and EMI measurements at 20 cm and 40 cm depths.

4.2. Solute Infiltration – 2nd Experiment

4.2.1. *Time-lapse σ_a data and estimation of σ_b distribution*

Figure 9 shows the σ_a data collected during the solute infiltration experiment. Again, as for the 1st experiment, both VCP and HCP modes show a relatively similar pattern of σ_a values with

499 ρ32 and ρ118 being the highest and lowest respectively. HCP mode shows higher values on
500 average compared to the VCP mode. Similarly, to the water infiltration experiment, σ_a increases
501 consistently during the first three hours of the experiment, then it does not change significantly or
502 consistently until the end of the experiment. Much higher ranges of σ_a variations were measured
503 in both VCP and HCP configurations, with σ_a values ranging in 20-200 and 50-250 mS m^{-1}
504 respectively.

505 Figure 10 depicts the σ_b evolution for the 2nd experiment, obtained by time-lapse inversion
506 of σ_a data. σ_a measurements and model response agrees fairly as shown in Fig. 9, however a slight
507 shift can be noticed in the ρ71- VCP mode between data and model response. The results show the
508 rapid evolution of the conductive zone to the soil profile shortly after the irrigation started. In
509 comparison to the obtained σ_b in the 1st experiment, the results reveal significantly higher soil
510 conductivity in topsoil but a much slower evolution. The conductivity of the top layer exceeds 300
511 mS m^{-1} shortly after the irrigation. The higher topsoil conductivity results from injection of high-
512 saline water (about 15 dS m^{-1}) that dramatically increases soil conductivity whereas the smaller
513 evolution of the conductive zone is caused by significantly slower concentration propagation into
514 the soil profile.

515

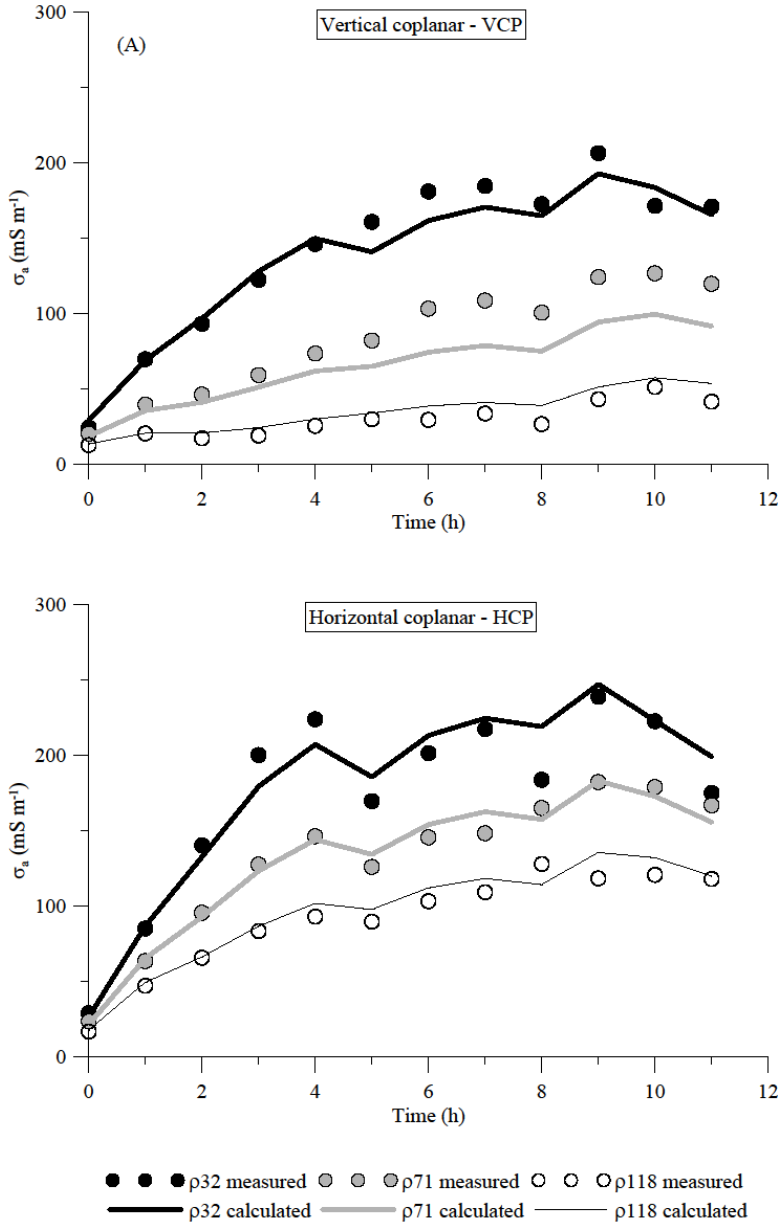

516

517 Figure 9: σ_a values observed during the solute infiltration experiment. (A) VCP, (B) HCP. The
518 symbols represent the measured data whereas the lines represent the values calculated after the
519 inversion.

520

521

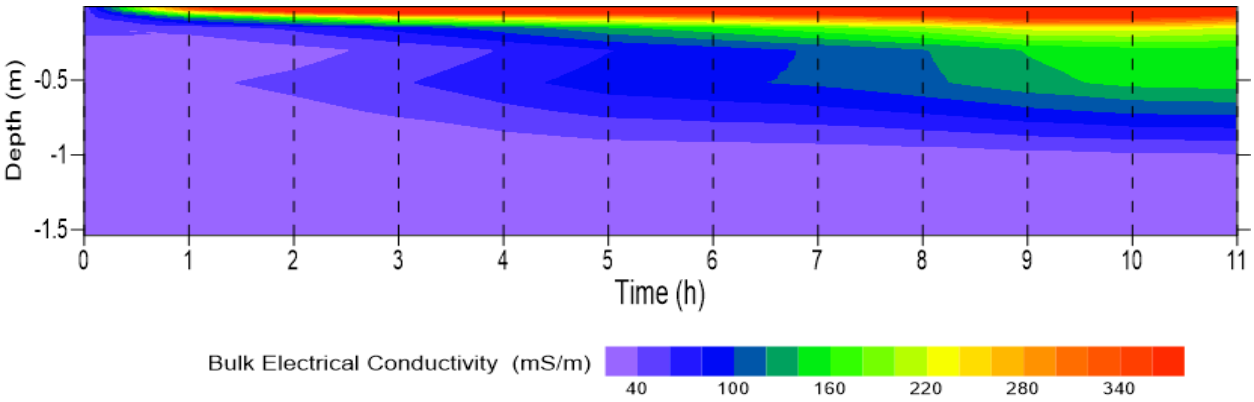

Figure 10. Time evolution of bulk electrical conductivity (σ_b) during the solute infiltration experiment.

4.2.2. *Comparison between TDR-based and EMI-based σ_b and [Cl^-] distributions*

Figure 11 shows the comparison between the σ_b values obtained by the TDR measurements and those obtained from the EMI inversion (Fig. 10) during the 2nd experiment. As discussed above, this comparison is to provide an insight into the potential of the EMI survey and inversion process in monitoring a solute transport experiment into a soil profile. The comparison shows a similar time pattern of σ_b variability, but in general the EMI model underestimates the σ_b obtained by TDR. The results of this comparison agree with the 1st experiment where, again, the EMI-based σ_b are lower compared to those measured by the TDR. In contrast to the 1st experiment, the differences between the two techniques and in terms of the absolute σ_b values are of minor concern. This could be due to the larger conductivity contrast that tracer introduced into the soil profile in the 2nd experiment which became easier to detect by using the EMI sensor. On the other hand, the TDR probes show more fluctuations in σ_b measurements, especially at 20 cm. We attribute these fluctuations to the smaller volume of investigation of the TDR probes which are very sensitive to the process taking place very close to the probe and, therefore, strongly influenced by small-scale heterogeneities.

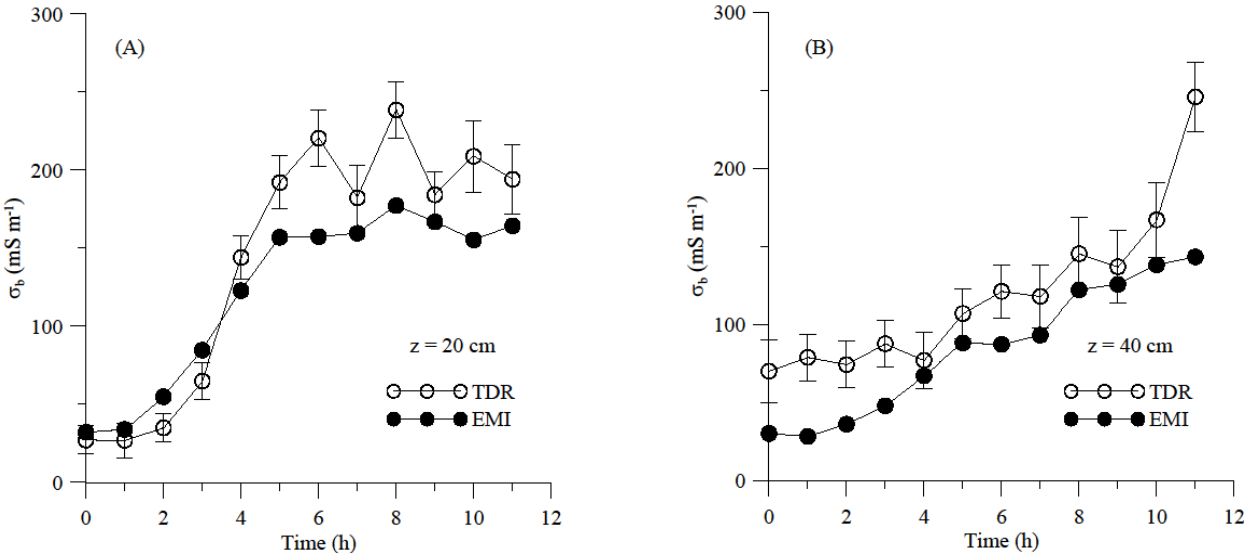

Figure 11. σ_b evolution estimated by TDR and EMI measurements at 20 cm (A) and 40 cm (B) depth.

The next step in the procedure allows us to determine the distribution of Cl^- concentrations by EMI sensors (Sect. 4.2.3.) used for estimating the longitudinal dispersivity of the two soil layers investigated. For the sake of comparison, TDR-based [Cl^-] distributions were obtained directly in the field from a direct measurement of the σ_b. As for the EMI-based Cl^- concentrations, a forward HYDRUS-1D simulation was carried out using the EMI-based hydraulic properties obtained from the 1st experiment and reported in Table 1 to estimate the water content distributions in correspondence with the EMI measurement times of the 2nd experiment. These water contents, combined with the available σ_b distribution obtained from the EMI inversion, allowed us to obtain the σ_w distributions (through the θ-σ_b-σ_w calibration relationship) for both depths and, consequently, the [Cl^-] distributions.

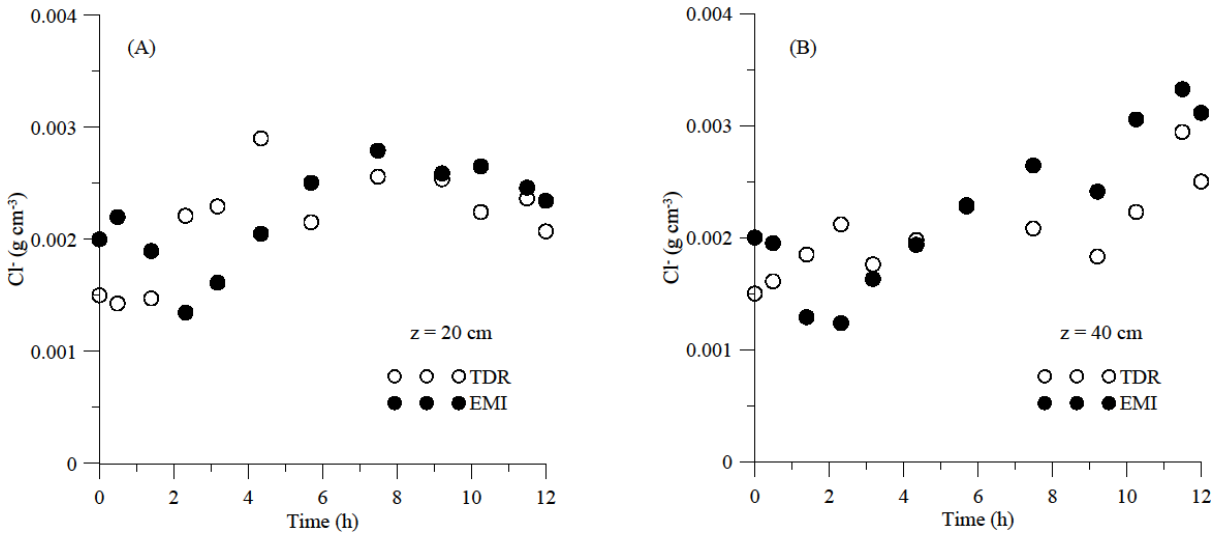

Figure 12. [Cl^-] distributions inferred from EMI and TDR measurements, at 20 (A) and 40 (B) cm depth.

Figure 12 shows the [Cl^-] distributions inferred from EMI compared to the TDR measurements. The comparison suggests a good agreement between the two time-series. The EMI-based concentrations underestimate – on average – the TDR-based ones by 4% and by 7% at 20 cm and 40 cm depths, respectively. The time evolution of the two data series reveals marked differences, as shown by the very different correlation: r = - 0.04 for the 20 cm depth and r = 0.70 for the 40 cm depth. The difference between the two data series at both depths can be mostly explained by the differences between σ_b distributions shown in Fig. 11. Additionally, another point of difference may arise from the assumption that the water content distribution obtained from the HYDRUS-1D simulation can be used as a substitute for the water content measurements, in order to obtain [Cl^-] from the EMI readings.

4.2.3. *Estimation of longitudinal dispersivity*

Inverse HYDRUS-1D simulations were conducted using concentration data provided by both the TDR and EMI results, in order to estimate the longitudinal dispersivity for both Ap and Bw horizons. The results are reported in the last row of Table 1. TDR-based and EMI-based procedures

provide similar values of λ. Specifically, for the Ap horizon, the obtained values agree with those frequently found in the literature for either large columns or field-measured dispersivity (e.g. Vanderborght and Vereecken, 2007; Coppola et al., 2011). The TDR and EMI-based estimation of dispersivity for the Bw horizon shows one order of magnitude lower values compared to the Ap horizon. These values are more consistent with values measured in the laboratory (Coppola et al., 2019). For column scale (undisturbed soil monoliths with a length > 30 cm), Vanderborght and Vereecken (2007) found values in the order of 10 cm. The same values were found by Coppola et al. (2011) at both plot and transect scales. Note in the Table 1 the high value of dispersivity used for the bedrock layer. This is consistent with the nature of the bedrock, which, as mentioned, is a fractured calcareous and highly conductive rock, which may well explain high dispersivity values.

5. FURTHER DISCUSSION ON THREE KEY POINTS OF THE PROPOSED APPROACH

Following, the discussion will focus on three major aspects of this research in terms of the choice of approach (uncoupled vs coupled), the suitability of EMI as a replacement for invasive sensors, and EMI-related sources of uncertainty.

5.1. **Uncoupled vs Coupled approach**

In hydro-geophysical studies there is an ample debate on this issue. Camporese et al. (2015), stated in their conclusions: “the relative merit of the coupled approach versus the uncoupled one cannot be assumed a priori and should be assessed case by case. As the information content of the geophysical data remains the same in both the coupled and uncoupled methods, the main difference is the approach taken in order to complement the information content and construct an ‘‘image’’

of the process". Based on the methodology proposed in this paper and the corresponding results, the following discussion aims to better clarify why we applied an uncoupled approach.

Let's refer to the vertical water infiltration process monitored by the EMI sensor during the 1st experiment and producing direct measurements of apparent electrical conductivity (σ_{a_meas}). In a coupled approach, the hydrological model is the starting point of the procedure. Guess values of hydraulic and dispersive parameters are initially fixed; thus, a hydrological simulation is carried out producing water content distributions along the soil profile, evolving over time. These water content distributions are converted to corresponding distributions of bulk electrical conductivity, σ_b, by using an empirical relationship (e.g. Binley et al., 2002). These σ_b distributions, in turn, are used as input in an EM forward modelling to produce the estimations of apparent electrical conductivity (σ_{a_est}). In this approach, the objective function involves the residuals ($\sigma_{a\_meas} - \sigma_{a\_est}$). This objective function is eventually minimised by optimising the hydraulic parameters in the hydrological model.

The main strength of this approach relies on the fact that no EMI inversion is required. Also, as discussed by Hinnell et al. (2010), the attractiveness of the coupled approach is that the hydrologic model may provide the physical context for a plausible interpretation of the geophysical measurements. Yet, this strength is counterbalanced by a weakness which is crucial in view of simplifying the experimental requirements of hydraulic characterization. Actually, an instrumental shift in EMI σ_a readings has been frequently observed when compared to other sources of measurements such as ERT data (von Hebel et al., 2014; 2019) or direct measurements of TDR (Dragonetti et al. 2018). In the context of a hydraulic parameter estimation procedure, this is a crucial point, as it means that EMI measurements do not immediately provide correct electrical conductivity distributions. Thus, the coupled approach always requires an independent dataset,

obtained by different sensors (e.g. ERT, TDR, sampling) to remove the shift in the EMI σ_a readings. Such a scheme would be contrary to the spirit of this paper, which mainly aims at minimising the sensors and the data necessary for in-situ soil hydraulic characterization.

In an uncoupled approach, the geophysical model is the starting point of the procedure. As a result of geophysical inversion, the σ_b distributions are derived, which are then converted to as many distributions of water content (θ_{meas}) through an empirical relationship, determined from laboratory analysis. Afterward, the hydrological model estimates water contents (θ_{est}), and the objective function, involving the residuals (θ_{meas}-θ_{est}), is eventually minimised by optimising the hydraulic parameters. The main weakness of this approach corresponds to the strength of the coupled approach. The uncoupled approach requires geophysical inversion, involving the uncertainty source coming from the ill-posedness problem. However, the main strength of the methodology we propose in this paper – a fast in-situ non-invasive method to estimate soil hydraulic and transport properties at plot scale – does not require preliminary removal of the (unknown) shift in the EMI readings by additional field measurements with other sensors. Conversely, the shift effect is implicitly kept in the σ_b distributions, from this in the measured water content distributions and finally included in the hydrological inversion. This allowed us to reveal the effects of technical limitations of the EMI sensor including the instrumental shift in EMI σ_a readings in the water content estimations and from this in the hydraulic properties' estimation. In the 1st experiment, by comparing the EMI-based water contents to the water contents coming from TDR, it was possible to see that the shift in the EMI readings produced quasi-parallel water content evolutions, thus meaning that the EMI shift is rather stable with water content change. Related to this, in terms of hydraulic properties, the shift simply results in scaled saturated water content. This may well be explained physically by just considering the parallel behaviour of the

638 water contents over time signifies similar water content changes over time. This is translated in
639 similar hydraulic conductivities, which in the van Genuchten-Mualem model means similar α and
640 n parameters, and thus water retention curves are simply scaled by the saturated water content
641 ratio.

642 As an additional benefit of an uncoupled approach, it allows for the sequential estimation of
643 parameters (from the upper to the lower horizon), which can reduce the problems of parameter
644 correlation and uniqueness. In this work, the parameters were estimated separately for each horizon
645 of the profile according to Abbaspour et al. (1999). This approach makes parameter estimation of
646 multi-layered profiles more feasible and accurate, however, this cannot be done within a coupled
647 model. If more than one layer has to be characterised, the coupled approach requires that all the
648 parameters have to be simultaneously optimised. This is because the electrical conductivity
649 distribution of the whole soil profile must be first simulated in order to generate required σ_{a_est} to
650 compare to σ_{a_meas} in the objective function.

651

652 **5.2. Suitability of EMI as a replacement for invasive sensors**

653 The proposed methodology for the estimation of vG-M parameters proved to be effective for
654 both Ap and Bw horizons. The overall EMI-based underestimation of θ did not impact the
655 hydraulic conductivity curves significantly, as the shape of hydraulic conductivity is mainly
656 explained by the θ variation and not of its absolute value. On the other hand, this underestimation
657 resulted in lower saturated water content which also appeared in the water retention curve. The
658 latter can be simply converted to more accurate water content distribution by direct measurement
659 of the actual saturated water content at the end of the experiment using TDR probes or even by
660 taking soil samples for laboratory weight.

In terms of the longitudinal dispersivity, λ, there was a very good agreement between EMI-based and TDR-based estimation for both Ap and Bw horizons. The finding results are also in very good agreement with previous in-situ and laboratory measurements. However, this method requires that the hydraulic properties of the investigated soil at the scale of concern be assessed prior to the application of this method to discriminate the contribution of water content and concentration in the EMI-based σ_b estimation.

5.3. EMI-related sources of uncertainty

The application of EMI for detailed investigation of the infiltration process has several limitations, apart from the potential instrumental drift of EMI sensor and the overall underestimation of water content and concentration, and requires further investigation. Resolving the wetting zone during the water injection is one source of uncertainty in this approach. The water content sharply decreases with depth in this zone to near the initial water content of the soil and causes dramatic resistivity variation. The limited number of σ_a measurements (total of 6) is not sufficient for recovering the sharp σ_b variability that takes place during the infiltration. In addition, a smoothness constraint was performed in the inversion process to stabilize the inversion process which further smooths the layer boundaries in this approach. Resolving the shallow bedrock interface at depth and beneath a conductive zone was also very challenging. This is because the sensitivity of the EMI signals is generally very limited over the resistive zone and the condition becomes much worse when the resistive zone (bedrock) is located beneath a conductive zone (tracer): the EMI response of the subsurface is dominated by the influence of the near-surface conductive zone. In addition, five of the six depths of investigation of the CMD Mini-Explorer are limited to the first 1 m, and, as a result, a lower resolution is expected at greater depths. This resulted in an even larger underestimation of soil conductivity on top of the bedrock and an

685 overestimation of bedrock conductivity in the close vicinity of soil. These findings from synthetic
686 studies and modelling field data are similar to those reported in Farzamian et al. (2021) due to the
687 similarity of the site, experiment, and the use of the same EMI sensor. Measuring σ_a at different
688 heights or using different EMI sensor with larger number of receivers such as CMD Mini-Explorer
689 6L enables us to collect more σ_a data to better resolve changes that occur over short depth
690 increments. To this aim, the EMI configuration and data survey can also be optimized using
691 optimization techniques such as machine learning based methods, given the specific survey goals
692 and independent knowledge of the subsurface electrical properties, as shown for example by van't
693 Veen et al. (2022).
694

695 ## 6. CONCLUSION

696 In this paper, we proposed a non-invasive in-situ method integrating EMI and hydrological
697 modelling to estimate soil hydraulic and transport properties at the plot scale. For this purpose, we
698 carried out two experiments involving 1) water infiltration and 2) solute transport over a 4 x 4 m
699 plot. The propagation of wetting front and solute concentration along the soil profile in the plot
700 was monitored using an EMI sensor (i.e. CMD mini-Explorer) and for the sake of procedure
701 evaluation Time Domain Reflectometry probes and tensiometers. Time-lapse apparent electrical
702 conductivity (σ_a) data obtained from the EMI sensor were inverted to estimate the evolution over
703 time of the vertical distribution of the bulk electrical conductivity (σ_b). The σ_b distributions were
704 converted to water content and solute concentration by using a standard laboratory calibration,
705 relating σ_b to water content (θ) and soil solution electrical conductivity (σ_w).

706 Based on the first water infiltration experiment, the soil water retention and hydraulic
707 conductivity curves were then obtained for two layers of the soil profile by an optimization

procedure minimizing the deviations between the numerical solution of the water infiltration experiment and the estimated water contents inferred from the EMI results. EMI-based hydraulic properties were very similar in shape to those obtained by TDR and tensiometers data. This shape-similarity allowed to convert the EMI-based hydraulic properties to the TDR-based ones by simply scaling them by the ratio of the saturated water content for both the soil layers considered. This was a crucial finding in this paper and was mainly ascribed to the fact that the water content changes over time detected by the EMI closely followed those observed by TDR. These EMI-based hydraulic properties were then used as input for hydrological modelling of the second solute transport experiment. This allowed discriminating water content and solute concentration components in the EMI σ_b distributions obtained during the second experiment. These concentrations were afterward used to estimate the dispersivity based on an inversion procedure minimizing the residuals of EMI-based concentration and those simulated by the hydrological model. The reliability of the EMI-based hydraulic properties allowed us to obtain estimations of the dispersivity comparable to those obtained by the same optimization procedure applied to the TDR data.

The overall results show the high potential of the EMI sensor to replace TDR and tensiometer probes in the assessment of soil hydraulic properties. In practice, one could monitor a relatively short infiltration experiment with an EMI sensor and use the water content estimations in an inversion procedure to estimate the hydraulic properties. The underestimated water content observed in the first experiment can be converted to more accurate water content distribution by direct measurement of the actual saturated water content at the end of the experiment using TDR probes or even by taking samples and laboratory measurements.

730 The EMI-based estimation of longitudinal dispersivity, λ agrees well with TDR-based
731 estimation as well as previous in-situ and laboratory measurements which suggests that the
732 proposed methodology can be used in the assessment of this parameter which is indeed an
733 important parameter in soil salinity simulations in salt-affected regions across the world. However,
734 estimating λ based on only a solute infiltration test is not feasible as the temporal variability of σ_b
735 is a function of both water content and concentration changes. We proposed the sequence of water
736 and solute infiltration tests to discriminate the contribution of the water content and the soil
737 solution electrical conductivity to the EMI-based σ_b.

738 Water irrigation and soil salinity management and thus hydrological investigations are usually
739 field and even large-scale challenges. The EM method is a non-invasive, fast, and cost-effective
740 technique, covering large areas in less time and at a lower cost. Although this study was limited to
741 a controlled experiment on a plot scale and a single study report, scaling up from plot scale to field
742 scale assessment might be feasible due to the method's potential for rapid data collection. More
743 investigations have to be conducted in this area to evaluate the potential of EMI sensors under
744 different soil conditions and within the larger 2D and 3D investigations to further address the
745 limitations of this methodology at different scales.

746

747 **ACKNOWLEDGMENTS**

748 This work was funded in the scope of the project SALTFREE: Salinization in irrigated areas: risk
749 evaluation and prevention [ARIMNet2, Grant agreement no. 618127], by the Italian Ministry of
750 Agricultural, Food and Forestry Policies [D.M. 28675/7303/15]. M. Farzamian was supported by

a contract within project SOIL4EVER [Increasing water productivity through the sustainable use of soils, PTDC/ASP-SOL/28796/2017].

REFERENCES

Abbasi, F., Šimůnek, J., Feyen, J., van Genuchten, M.T., and Shouse, P.T.: Simultaneous inverse estimation of soil hydraulic and solute transport parameters from transient field experiments: Homogeneous soil. Transactions of the ASAE 46(4): 1085, 2003.

Abbaspour, K.C., Sonnleitner, M., and Schulin, R.: Uncertainty in estimation of soil hydraulic parameters by inverse modeling: example lysimeter experiments. Soil Sci. Soc. Am. J. 63, 501–509, 1999.

Archie, G.E.: The electrical resistivity log as an aid in determining some reservoir characteristics. Transactions of the AIME 146(01): 54–62, 1942.

Basile, A., Coppola, A., De Mascellis, R., and Randazzo, L.: Scaling Approach to Deduce Field Unsaturated Hydraulic Properties and Behavior from Laboratory Measurements on Small Cores, Vadose Zone J., 5, 1005–1016, https://doi.org/10.2136/vzj2005.0128, 2006.

Binley, A., Cassiani, G., Middleton, R., and Winship, P.: Vadose zone flow model parameterisation using cross-borehole radar and resistivity imaging. Journal of Hydrology 267(3–4): 147–159, https://doi.org/10.1016/S0022-1694(02)00146-4, 2002.

Bouksila, F., Persson, M., Bahri, A., and Berndtsson, A.: Electromagnetic induction prediction of soil salinity and groundwater properties in a Tunisian Saharan oasis. Hydrological sciences journal 57(7): 1473–1486, https://doi.org/10.1080/02626667.2012.717701. 2012.

Camporese, M., Cassiani G., Deiana R., Salandin P., and Binley A.: Coupled and uncoupled hydrogeophysical inversions using ensemble Kalman filter assimilation of ERT-monitored tracer test data, Water Resour. Res., 51, 3277–3291, doi:10.1002/2014WR016017, 2015

Caputo, M.C., De Carlo, L., Masciopinto, C., and Nimmo, J.R.: Measurement of field-saturated hydraulic conductivity on fractured rock outcrops near Altamura (Southern Italy) with an adjustable large ring infiltrometer, Environ. Earth Sci., 60, 583–590, https://doi.org/10.1007/s12665-009-0198-y, 2010.

Caputo M.C., Maggi S., and Turturro A.C.: Calculation of Water Retention Curves of Rock Samples by Differential Evolution, in: Engineering Geology for Society and Territory, edited by Lollino G., Manconi A., Guzzetti F., Culshaw M., Bobrowsky P., Luino F. (eds), Volume 5, Springer, Cham, https://doi.org/10.1007/978-3-319-09048-1, 2015.

Coppola, A., Comegna, A., Dragonetti, G., Dyck, M., Basile, A., Lamaddalena, N., Kassab, M., and Comegna, V.: Solute transport scales in an unsaturated stony soil, Adv. Water Resour., 34, 747–759, https://doi.org/10.1016/j.advwatres.2011.03.006, 2011.

Coppola, A., Gerke, H., Comegna, A., Basile, A., and Comegna, V.: Dual-permeability model for

flow in shrinking soil with dominant horizontal deformation. Water Resources Research, Vol. 48, W08527, doi:10.1029/2011WR011376, 2012.

Coppola, A., Smettem, K., Ajeel, A., Saeed, A., Dragonetti, G., Comegna, A., Lamaddalena, N., and Vacca, A.: Calibration of an electromagnetic induction sensor with time-domain reflectometry data to monitor rootzone electrical conductivity under saline water irrigation, Eur. J. Soil Sci., 67, 737–748, https://doi.org/10.1111/ejss.12390, 2016.

Coppola, A., Dragonetti, G., Comegna, A., Lamaddalena, N., Caushi, B., Haikal, M. A., and Basile, A.: Measuring and modeling water content in stony soils, Soil and Tillage Research, 128, 9–22, https://doi.org/10.1016/j.still.2012.10.006, 2013.

Coppola, A., Dragonetti, G., Sengouga, A., Lamaddalena, N., Comegna , A., Basile, A., Noviello, N., and Nardella, L.: Identifying Optimal Irrigation Water Needs at District Scale by Using a Physically Based Agro-Hydrological Model. Water 11(4). https://doi.org/10.3390/w11040841, 2019.

Coppola, A., Chaali, N., Dragonetti, G., Lamaddalena, N., and Comegna, A.: Root uptake under non-uniform root-zone salinity, Ecohydrology, 8, 1363–1379, https://doi.org/10.1002/eco.1594, 2015.

Corwin, D. L., and Lesch, S. M.: Apparent soil electrical conductivity measurements in agriculture, Comput. Electron. Agr., 46, 11–43, https://doi.org/10.1016/j.compag.2004.10.005, 2005.

Dane, J. H., & Topp, C. G. (Eds.). (2020). Methods of soil analysis, Part 4: Physical methods (Vol. 20). John Wiley & Sons.

Deidda, G.P., Fenu, C., and Rodriguez, G.: Regularized solution of a nonlinear problem in electromagnetic sounding, Inverse Probl., 30, 125014, https://doi.org/10.1088/0266-5611/30/12/125014, 2014.

Dragonetti, G., Comegna, A., Ajeel, A., Deidda, G. P., Lamaddalena, N., Rodriguez, G., Vignoli, G., and Coppola, A.: Calibrating electromagnetic induction conductivities with time-domain reflectometry measurements, Hydrol. Earth Syst. Sci., 22, 1509–1523, https://doi.org/10.5194/hess-22-1509-2018, 2018.

Ellsworth, T.R., Shaouse, P.J., Jobes, J.A., Fargerlund, J., and Skaggs, T.H.: Solute transport in unsaturated soil: Experimental design, parameter estimation, and model discrimination. Soil Science Society of America Journal 60(2): 397–407, https://doi.org/10.2136/sssaj1996.03615995006000020010x, 1996.

Farzamian, M., Paz, M. C., Paz, A. M., Castanheira, N. L., Gonçalves, M. C., Monteiro Santos, F. A., and Triantafilis, J.: Mapping soil salinity using electromagnetic conductivity imaging–A comparison of regional and location-specific calibrations, Land. Degrad. Dev., 30, 1393–1406, https://doi.org/10.1002/ldr.3317, 2019a.

Farzamian, M., Ribeiro, J.A., Monteiro Santos, F.A., Khalil M.A.: Application of Transient Electromagnetic and Audio-Magnetotelluric Methods for Imaging the Monte Real Aquifer in Portugal. Pure Appl. Geophys, https://doi.org/10.1007/s00024-018-2030-7, 2019b.

Farzamian, M., Autovino, D., Basile, A., De Mascellis, R., Dragonetti, G., Monteiro Santos, F., Binley, A., and Coppola, A.: Assessing the dynamics of soil salinity with time-lapse inversion of electromagnetic data guided by hydrological modelling, Hydrol. Earth Syst. Sci., 25, 1509–

1527, https://doi.org/10.5194/hess-25-1509-2021, 2021.

Groh, J., Stumpp, C., Lücke, A., Pütz, T., Vanderborght, J., Vereecken, H.: Inverse estimation of soil hydraulic and transport parameters of layered soils from water stable isotope and lysimeter data. Vadose Zone Journal 17(1): 1–19, https://doi.org/10.2136/vzj2017.09.0168, 2018.

Gómez Flores, J.L., Ramos Rodríguez, M., González Jiménez, A., Farzamian, M., Herencia Galán, J.F., Salvatierra Bellido, B., Cermeño Sacristan, P., and Vanderlinden, K.: Depth-Specific Soil Electrical Conductivity and NDVI Elucidate Salinity Effects on Crop Development in Reclaimed Marsh Soils. Remote Sens., 14, 3389. https://doi.org/10.3390/rs14143389, 2022.

Hansen, S., Abrahamsen, P., Petersen, C.T., Styczen, M., 2012. Daisy: model use, calibration and validation. Trans. ASABE 55, 1315–1333.

Hendrickx, J.M.H., Borchers, B., Corwin, D.L., Lesch, S.M., Hilgendorf, A.C., and Schlue, J.: Inversion of soil conductivity profiles from electromagnetic induction measurements, Soil Sci. Soc. Am. J., 66, 673–685, https://doi.org/10.2136/sssaj2002.6730, 2002.

Hinnell, A.C., Ferre, T.P.A., Vrugt, J.A., Huisman, J.A., Moysey, S., Rings, J., and Kowalsky, M.B.: Improved extraction of hydrologic information from geophysical data through coupled hydrogeophysical inversion. J. Water Resour. Res. 46, W00D40, https://doi.org/10.1029/2008WR007060, 2010.

Huang, J., Monteiro Santos, F. A., and Triantafilis, J.: Mapping soil water dynamics and a moving wetting front by spatiotemporal inversion of electromagnetic induction data, Water Resour. Res., 52, 9131–9145, https://doi.org/10.1002/2016WR019330, 2016.

Inoue, M., Šimuunek, J., Shiozawa, S., and Hopmans, J.W.: Simultaneous estimation of soil hydraulic and solute transport parameters from transient infiltration experiments. Advances in Water Resources 23(7): 677–688, https://doi.org/10.1016/S0309-1708(00)00011-7, 2000.

Kaufman, A.A., and Keller, G.V.: Frequency and Transient Sounding Methods Geochemistry and Geophysics. Elsevier Science Ltd, New York, 1983.

Kemna, A., Vanderborght, J., Kulessa, B., and Vereecken, H.: Imaging and characterization of subsurface solute transport using electrical resistivity tomography (ERT) and equivalent transport models. Journal of hydrology 267(3–4): 125–146, https://doi.org/10.1016/S0022-1694(02)00145-2, 2002.

Kroes, J.G., van Dam, J.C., Bartholomeus, R.P., Groenendijk, P., Heinen, M., Hendriks, R. F.A., Mulder, H.M., Supit, I., van Walsum, P.E.V., 2017. SWAP version 4; Theory description and user manual. Wageningen, Wageningen Environmental Research, Report 2780. 244 pp.

Lavoué, F., van der Kruk, J., Rings, J., André, F., Moghadas, D., Huisman, J.A., Lambot, S., Weihermüller, L., Vanderborght, J., and Vereecken, H..: Electromagnetic induction calibration using apparent electrical conductivity modelling based on electrical resistivity tomography, Near Surf. Geophys., 8, 553–561, 2010.

Malicki, M. A. and Walczak, R. T.: Evaluating soil salinity status from bulk electrical conductivity and permittivity, Eur. J. Soil Sci., 50, 505–514, https://doi.org/10.1046/j.1365-2389.1999.00245.x, 1999.

McLachlan, P., Blanchy, G., and Binley, A.: EMagPy: Open-source standalone software for processing, forward modeling and inversion of electromagnetic induction data. Computers &

Geosciences. https://doi.org/10.1016/j.cageo.2020.104561, 2020.

McNeill, J.D.: Electromagnetic Terrain Conductivity Measurement at Low Induction Numbers. Geonics Limited, Ontario, Canada, Technical note TN-06 1–15, 1980.

Moghadas, D.: Probabilistic Inversion of Multiconfiguration Electromagnetic Induction Data Using Dimensionality Reduction Technique: A Numerical Study, Vadose Zone J., 18, 1–16, https://doi.org/10.2136/vzj2018.09.0183, 2019.

Monteiro Santos, F. A.: 1D laterally constrained inversion of EM34 profiling data, J. Appl. Geophys., 56, 123–134, https://doi.org/10.1016/j.jappgeo.2004.04.005, 2004.

Paz, M. C., Farzamian, M., Paz, A. M., Castanheira, N. L., Gonçalves, M. C., and Monteiro Santos, F.: Assessing soil salinity using time-lapse electromagnetic conductivity imaging, SOIL, 6, 499–511, https://doi.org/10.5194/soil-6-499-2020, 2020.

Robinson, D.A., Jones, S.B., Wraith, J.M., Or, D., and Friedman, S.P..: A Review of Advances in Dielectric and Electrical Conductivity Measurement in Soils Using Time Domain Reflectometry. Vadose Zone Journal 2: 444–475. doi: 10.2136/vzj2003.4440, 2003.

Saeed A., Comegna, A., Dragonetti, G., Lamaddalena, N., and Coppola, A.: Soil surface electrical conductivity estimated by TDR and EMI sensors: Accounting for the different sensor observation volumes, J. of Agricultural Engineering. Vol XLVIII, doi:10.4081/jae.2017.716, 2017.

Sasaki, Y.: Full 3-D inversion of electromagnetic data on PC. Journal of Applied Geophysics 46(1): 45–54. doi: 10.1016/S0926-9851(00)00038-0, 2001.

Severino G, Comegna A., Coppola A., Sommella A., Santini A.: Stochastic analysis of a field-scale unsaturated transport experiment, Advances in Water Resources, doi:10.1016/j.advwatres.2010.09.004, 2010.

Šimůnek, J., Angulo-Jaramillo, R., Schaap, M.G., Vandervaere, J.P., and van Genuchten, M.T.: Using an inverse method to estimate the hydraulic properties of crusted soils from tension-disc infiltrometer data. Geoderma 86(1): 61–81. doi: 10.1016/S0016-7061(98)00035-4, 1998a.

Šimůnek, J., Sejna, M., van Genuchten, M.T., Šimuunek, J., and Šejna, M.: HYDRUS-1D. Simulating the one-dimensional movement of water, heat, and multiple solutes in variably-saturated media, version 2, 1998b.

Sisson, J., and van Genuchten, M.Th.: An improved analysis of gravity drainage experiments for estimating the unsaturated soil hydraulic functions. Water Resour. Res. 27:569–575, 1991.

Singha, K., and Gorelick, S.M.: Saline tracer visualized with three-dimensional electrical resistivity tomography: Field-scale spatial moment analysis. Water Resources Research 41(5). https://doi.org/10.1029/2004WR003460, 2005.

Topp, G.C., Davis, J.L., and Annan, A.P.: Electromagnetic determination of soil water content: Measurements in coaxial transmission lines. Water Resources Research, 16(3), 574-582, 1980.

Vanderborght J., and Vereecken, H.: Review of Dispersivities for Transport Modeling in Soils. Vadose Zone Journal 6(1) doi:10.2136/vzj2006.0096, 2007.

Watson, K. K., 1966. An instantaneous profile method for determining the hydraulic conductivity of unsaturated porous materials, Water Resour. Res., 2, 709–715, 1966.

van Genuchten, M. T.: A closed-form equation for predicting the hydraulic conductivity of unsaturated soils, Soil Sci. Soc. Am. J., 44, 892–898, 1980.

van Genuchten, M.T., Leij, F.J. and Wu, L.: Characterization and measurement of the hydraulic properties of unsaturated porous media (parts 1 and 2). Proceedings of the International Workshop, Riverside, Calif., 22--24 Oct, 1999.

van't Veen, K.M., Ferré, T.P.A., Iversen, B.V., and Børgesen, C.D.: Using machine learning to predict optimal electromagnetic induction instrument configurations for characterizing the shallow subsurface, Hydrol. Earth Syst. Sci., 26, 55–70, https://doi.org/10.5194/hess-26-55-2022, 2022.

Visconti, F., and de Paz, J.M.: Sensitivity of soil electromagnetic induction measurements to salinity, water content, clay, organic matter and bulk density. Precision Agriculture, 2021,1-19, doi: 10.1007/s11119-021-09798-8, 2021.

von Hebel, C., Rudolph, S., Mester, A., Huisman, J. A., Kumbhar, P., Vereecken, H., and van der Kruk, J.: Three-dimensional imaging of subsurface structural patterns using quantitative large-scale multiconfiguration electromagnetic induction data, Water Resour. Res., 50, 2732–2748, https://doi.org/10.1002/2013WR014864, 2014.

von Hebel, C., van der Kruk, J., Huisman, J.A., Mester, A., Altdorff, D., Endres, A.L., Zimmermann, E., Garré, S., and Vereecken, H.: Calibration, Conversion, and Quantitative Multi-Layer Inversion of Multi-Coil Rigid-Boom Electromagnetic Induction Data. Sensors, 19, 4753. https://doi.org/10.3390/s19214753, 2019.

Wessolek, G., Plagge, R. Leij, F.J., and van Genuchten, M.T..: Analysing problems in describing field and laboratory measured soil hydraulic properties. Geoderma 64(1–2): 93–110. https://doi.org/10.1016/0016-7061(94)90091-4, 1994.

Whalley, W. R., Binley, A. M., Watts, C. W., Shanahan, P., Dodd, I. C., Ober, E. S., Ashton, R. W., Webster, C. P., White, R. P., and Hawkesford, M. J.: Methods to estimate changes in soil water for phenotyping root activity in the field, Plant Soil, 415, 407–422. https://doi.org/10.1007/s11104-016-3161-1, 2017.

Zare, E., Li, N., Khongnawang, T., Farzamian, M., and Triantafilis, J.: Identifying Potential Leakage Zones in an Irrigation Supply Channel by Mapping Soil Properties Using Electromagnetic Induction, Inversion Modelling and a Support Vector Machine, Soil Syst., 4, 25, https://doi.org/10.3390/soilsystems4020025, 2020.